Int J Adv Manuf Technol (2007) 35:280–292
DOI 10.1007/s00170-006-0721-1

ORIGINAL ARTICLE

Clad height control in laser solid freeform fabrication using a feedforward PID controller

Alireza Fathi · Amir Khajepour · Ehsan Toyserkani · Mohammad Durali

Received: 10 April 2006 / Accepted: 7 July 2006 / Published online: 6 October 2006

Abstract In this paper, a feedforward proportional-integral-derivative (PID) controller is developed to effectively control the clad height in laser solid freeform fabrication (LSFF). The scanning velocity is selected as the input control variable and the clad height is chosen as the output. A novel knowledge-based Hammerstein model, including a linear dynamic and a nonlinear memoryless block, is developed, and its parameters are identified offline using experimental data. The architecture of the controller consists of a PID and a feedforward module, which is the inverse of the identified model. The advantage of adding a feedforward path to the PID controller is evaluated experimentally, in which the results show a lower overshoot and faster response times. Also, the performance of the controller is verified in the presence of geometrical disturbances, as well as in the fabrication of a nonplanar part.

Keywords Laser solid freeform fabrication · Feedforward control · Feedback control · Clad height control · Rapid prototyping

A. Fathi · A. Khajepour · E. Toyserkani (✉)
Department of Mechanical and Mechatronics Engineering,
University of Waterloo,
Waterloo, ON N2L 3G1, Canada
e-mail: etoyserk@uwaterloo.ca

A. Fathi
e-mail: afathi@engmail.uwaterloo.ca

A. Khajepour
e-mail: akhajepour@uwaterloo.ca

M. Durali
Department of Mechanical Engineering,
Sharif University of Technology,
11365-8639 Tehran, Iran
e-mail: durali@sharif.edu

1 Introduction

Laser solid freeform fabrication (LSFF) is an advanced laser material deposition technique which has many applications, such as coating, tool repair, low-volume manufacturing, rapid prototyping, and the fabrication of functionally graded materials (FGM) [1, 2]. LSFF offers a revolutionary layered manufacturing and prototyping technique. The integration of LSFF technology with a three-dimensional computer-aided design (CAD) solid model, which is sliced into many layers, provides the ability to fabricate complex functional components without intermediate steps.

For all of the above applications, depositing a clad (deposited layer) with a desired thickness is required. With an open-loop system, the clad height/shape may vary significantly because of fluctuations in system parameters, as well as disturbances in the work environment. For example, during the process, the overall temperature of the part increases, resulting in an increase in the laser power absorption and, subsequently, in the melt pool size. Another example that shows the necessity of a closed-loop system is the application of LSFF in the rapid prototyping of parts using the adaptive slicing technique. The adaptive slicing technique calls for varying clad heights over the trajectories.

Despite numerous advantages of the closed-loop LSFF process, there are limited studies and published research on the design and implementation of closed-loop controls for the LSFF process. Hu and Kovacevic [3] designed a proportional-integral-derivative (PID) controller for controlling the melt pool area and the heat input via changing the laser power. Mazumder et al. [4] proposed a bang-bang controller using the laser shutter to control the clad height. In their approach, the laser shutter is closed if the clad height exceeds a preset value. Liu and Li [5] studied the

control of laser direct metal deposition for improving the dimensional accuracy and surface finish of the clad. They used motion parameters such as laser scanning speed, stand-off distance, and laser approach orientation as the controlling parameters. In this study, no detail is given on the type of the controller nor the control algorithm. Hua and Choi [6] proposed a fuzzy-logic-based controller for LSFF. The proposed closed-loop system could follow the desired clad height by varying the laser power as the control variable. Toyserkani et al. [7] developed a Hammerstein-Wiener model and used a PID controller to adjust the laser power to control the clad height.

In the majority of the above-mentioned works, the laser power has been selected as the control variable. Furthermore, the details of the controllers have not been disclosed. The LSFF process can be controlled using different control parameters, including powder flow rate, laser power, and scanning speed. In general, the response time of lasers (i.e., CO_2 and Nd:YAG) and powder feeders to any changes is relatively slow and, as a result, their use in a closed-loop control systems can generate a delay in the control loop. In contrast, the response times of motion systems are fast and are more effective in developing a closed-loop LSFF process.

In this paper, a vision-based closed-loop LSFF system is presented. The proposed controller regulates the scanning speed such that the clad height follows the desired value. The controller is designed based on a semi-empirical model, which is a nonlinear parametric model extracted from the governing equations (i.e., the heat and mass balance equations). The parameters associated with the model structure are identified using experimental data. The controller structure includes a PID and a feedforward controller to not only improve the system response time, but also to compensate for error and disturbance rejection. The experimental results show that the proposed method can effectively control the clad height with excellent accuracy.

2 LSFF process model

Figure 1 shows a schematic of the LSFF process, in which a moving laser beam melts a thin layer of the substrate, together with powder particles, to form a clad. The powder is sprayed into the melt pool by a lateral nozzle and solidifies as the laser beam moves away. Depending on the level of laser power, laser beam velocity, powder flow rate, and the type of materials, a clad with a specific geometry is formed.

The first step in the design of a model-based controller is the development of a model which accurately shows the actual physical behavior of the system. Due to the complexity of the governing equations (i.e., heat transfer and fluid flow) and their boundary conditions, finding a model that relates the clad geometry to the process inputs is difficult. To overcome these complexities, several authors have used system identification techniques to arrive at a dynamic model for different methods of laser material processing. Römer et al. [8] found a linear dynamic model for the laser alloying process when the scanning velocity or laser power was selected as the input and the melt pool temperature as the output.

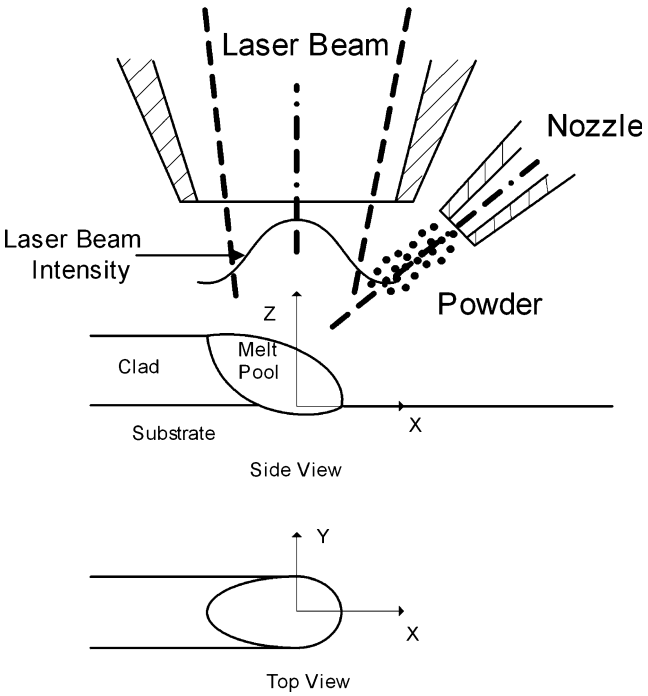

Fig. 1 Schematic of the laser solid freeform fabrication (LSFF) process

Since the effectiveness of a process control strongly relies on the system model accuracy, in this paper, a novel semi-empirical model is developed. The proposed model relates the clad height as a nonlinear dynamic function to the scanning velocity.

The structure of the proposed model is similar to a Hammerstein model [9]. This model is a type of block-oriented nonlinear model consisting of a memoryless nonlinear block followed by a linear dynamic submodel. This model assumes a separation between the nonlinearity and the dynamics of the process. Therefore, the linear dynamic block illustrates the transient response and the nonlinear block predicts the steady-state amplitude of the system.

LSFF is a thermal process and, according to the governing equations and the experimental tests, its dynamic response can be approximated with a first-order system [1, 8]. Figure 2 shows an experimental step response of the system to a change in velocity. As this figure shows, the system response does not have overshoot and its transient behavior can be

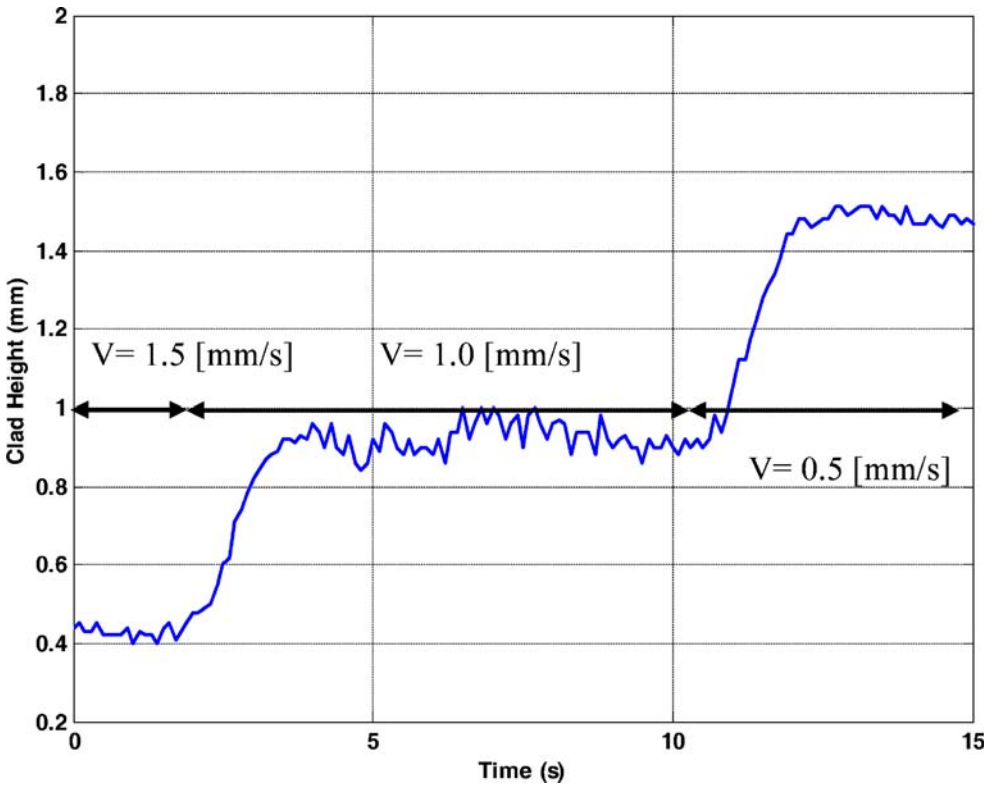

Fig. 2 Experimental result of the plant output with varying scanning velocity

approximated with a first-order dynamic system. Therefore, the system model is chosen as shown in Fig. 3. According to this figure, the process model, which includes a memoryless block followed by a dynamic block, can be expressed as:

$$\tau\dot{h} + h = h_0 \tag{1a}$$

$$h_0 = f(v) \tag{1b}$$

where h is the clad height [m], v is the scanning velocity [m/s], τ is the system time constant [s], and h_0 is a dummy variable.

To avoid the redundancy, the dynamic block is selected such that its gain is equal to 1. Therefore, at steady-state response, h will be equal to h_0. For finding the nonlinear memoryless block $f(\cdot)$, we know that h_0 represents the steady-state value of the clad height at scanning speed v.

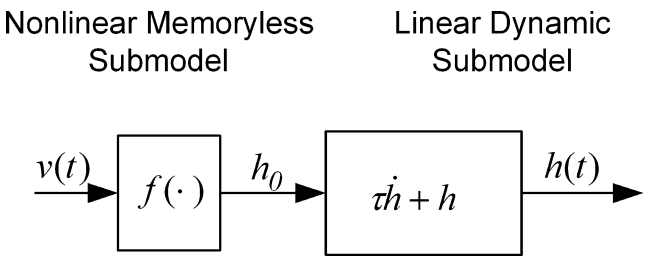

Fig. 3 Structure of the proposed model

In the LSFF process, the steady-state value of the clad height is related to the velocity through the mass balance equation, which means that the amount of powder that enters into the melt pool in time dt is equal to the mass of the clad that is created at the same time. According to Fig. 4, if A_{cl} is the clad cross-sectional area [m^2], and the substrate moves with a constant velocity v, then the mass of the clad that is created at time dt is $(\rho A_{cl} v)dt$ and the amount of the powder that enters is $\left(\eta\dot{m}\right)dt$, where ρ is the powder density [$\mathrm{kg/m}^3$], η is the powder catchment efficiency [%], and $\dot{m}$ is the powder flow rate [kg/s]. Based on the mass balance principle, these two quantities should be equal and, therefore, the following equation is obtained:

$$\rho A_{cl} v = \eta\dot{m} \tag{2}$$

With the assumption of a parabolic shape for the upper side of the clad (see Fig. 4), the clad cross-sectional area A_{cl} can be derived as:

$$A_{cl} = \frac{2}{3} h_0 w_0 \tag{3}$$

where h_0 and w_0 are the steady-state values of the clad height and the clad width [m], respectively.

By substituting Eq. 3 into Eq. 2, the steady-state value of the clad height is obtained as:

$$h_0 = \frac{3}{2}\frac{\eta\dot{m}}{\rho w_0 v} \tag{4}$$

Fig. 4 Proposed clad geometry

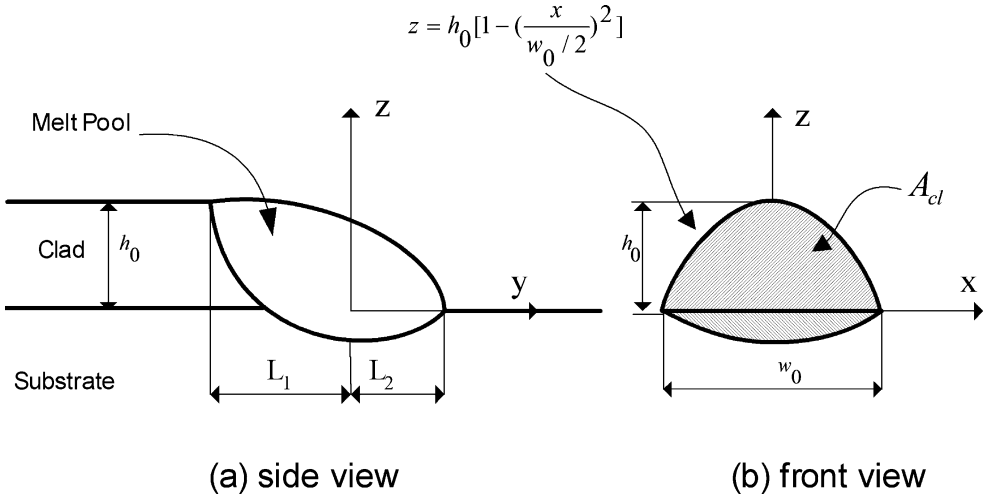

By substituting Eq. 4 into Eq. 1a, the process dynamic model is obtained as:

$$\tau\dot{h} + h = \frac{3}{2}\frac{\eta\dot{m}}{\rho w_0 v} \tag{5}$$

The parameter η indicates the amount of powder that is caught by the melt pool. Since at higher clad heights the melt pool size is larger, the powder catchment efficiency increases, and vice versa. Experimental results have shown that the powder catchment efficiency η is a geometrical factor and is proportional to the ratio of the melt pool surface and the section of the powder jet both projected onto the same plane [10]. Figure 5 shows a schematic view of the melt pool and the powder jet cross-sections. According to this figure, the ratio of these two planes can be approximated by the following index:

$$\eta \propto \frac{A_{meltpool}}{A_{powder\,jet}} \propto \left(\frac{L_2}{d_p}\right)^n = k\left(\frac{L_2}{d_p}\right)^n \tag{6}$$

where L_2 is the projected melt pool length L_1 (see Fig. 5) on the powder jet plane [m], d_p is the powder jet diameter [m], n is an unknown parameter which is experimentally shown to be around 2, and k is an unknown proportional parameter.

Parameter L_2 can be written as a function of the laser beam diameter d_b and the clad height as:

$$\beta = tan^{-1}\left(\frac{h}{d_b}\right) \tag{7}$$

$$L_1 = \frac{d_b}{cos\,\beta} \tag{8}$$

$$L_2 = L_1\,cos\,(\alpha - \beta) \tag{9}$$

where α is the angle between the nozzle and the laser beam.

By substituting Eqs. 7–9 into Eq. 6, a nonlinear function for the powder catchment efficiency is obtained as:

$$\eta = k\left(\frac{d_b}{d_p}(1 + \frac{h}{d_b}\,tan\,\alpha)\,cos\,\alpha\right)^n \tag{10}$$

By substituting Eq. 10 into Eq. 5, the parametric model of the process is formed as:

$$\tau\dot{h} + h = \frac{3}{2}\frac{\dot{m}}{\rho w_0}\left(\frac{d_b}{d_p}(1 + \frac{h}{d_b}\,tan\,\alpha)\,cos\,\alpha\right)^n \frac{k}{v} \tag{11}$$

In Eq. 11, the parameters τ, k, and n are unknown and should be identified experimentally. For the identi-

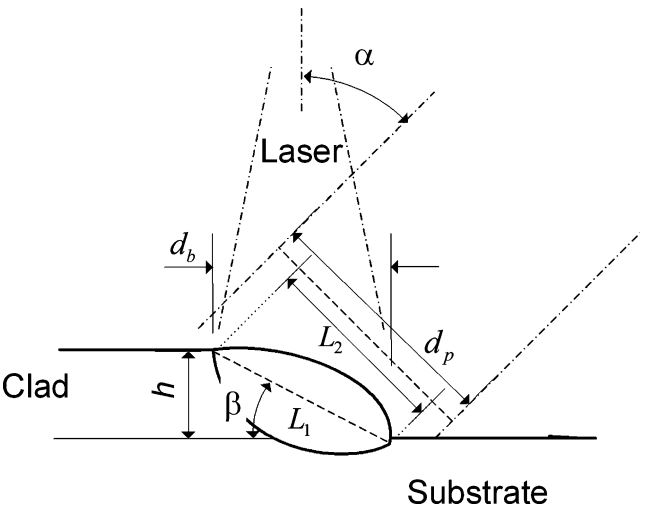

Fig. 5 Schematic view of the melt pool, the powder jet, and the laser beam

fication of the model parameters, we use a discrete form of Eq. 11 as:

$$h(t+1) = (1 - \frac{T_s}{\tau} h(t) + \frac{3}{2} \frac{\dot{m} T_s}{\rho w_0} \times \left(\frac{d_b}{d_p} (1 + \frac{h(t)}{d_b} tan\,\alpha) cos\,\alpha \right)^n (\frac{k}{\tau}) \frac{1}{v(t)} \quad (12)$$

where T_s is the sampling period [s] and t is the sample number.

Equation 11 is a nonlinear function of the parameters τ, k, and n. In order to avoid the application of nonlinear optimization techniques, in this paper, the parameter n is assumed to be constant. With this assumption, Eq. 12 will be linear with respect to $(1-T_s/\tau)$ and (k/τ); hence, Eq. 12 can be presented as a linear regression as:

$$h(t+1) = \boldsymbol{\theta}^T \varphi \quad (13)$$

where $\boldsymbol{\theta}$ are the model parameters and φ are the regression vectors, which are defined as:

$$\boldsymbol{\theta} = [\,\theta_1\ \theta_2\,]^T = \left[\left(1 - \tfrac{T_s}{\tau}\right) \frac{k}{\tau} \right]^T \quad (14)$$

$$\varphi = [\,\varphi_1\ \varphi_2]^T = \left[h(t) \frac{3}{2} \frac{\dot{m} T_s}{\rho w_0} \left(\frac{d_b}{d_p} \left(1 + tan\,\alpha \frac{h(t)}{d_b} \right) cos\,\alpha \right)^n \frac{1}{v(t)} \right]^T \quad (15)$$

Using the experimental results and the recursive least-squares (RLS) method, the model parameters are identified offline. The experimental tests are selected at different processing parameters; therefore, a domain is obtained for each of the model parameters, which can be expressed as:

$$\tau_{min} \le \tau \le \tau_{max} \quad (16a)$$

$$k_{min} \le k \le k_{max} \quad (16b)$$

3 Controller design

The block diagram of the proposed control system is shown in Fig. 6. Based on this figure, the controller consists of a feedforward path and a conventional PID feedback loop.

The feedforward controller is designed on the basis of the identified model in the previous section and produces a control action appropriate for the desired setpoint. The feedforward controller takes advantage of the known desired clad height to compute an appropriate control action that is injected in the closed-loop system. Since achieving both good tracking and disturbance rejection with a PID feedback controller is very difficult, by adding a feedforward control, as shown in Fig. 6, a suitable input can be computed using the system model and the desired output. This input is applied directly to the system instead of the PID feedback controller computing it based on the tracking error.

According to the controller structure (see Fig. 6), the feedforward path should approximate the inverse dynamics of the LSFF process. Using the proposed model, Eq. 11, this inverse, which is, in fact, the feedforward velocity v_{ff} is computed as:

$$v_{ff} = \frac{\widehat{k} g(h_d)}{\widehat{\tau} \dot{h}_d + h_d} \quad (17a)$$

$$g(h_d) = \frac{3}{2} \frac{\dot{m}}{\rho w_0} \left(\frac{d_b}{d_p} (1 + tan\,\alpha \frac{h_d}{d_b}) cos\,\alpha \right)^n \quad (17b)$$

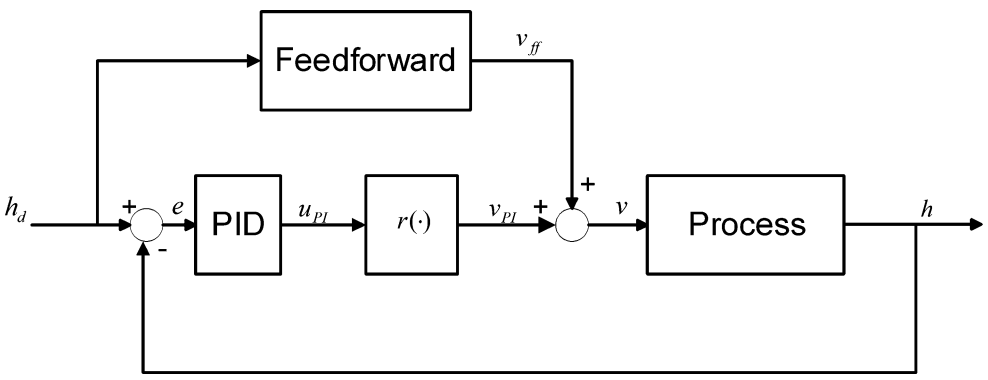

Fig. 6 Block diagram of the proposed closed-loop process

where h_d is the desired clad height $\hat{\tau}$ and $\hat{k}$ are the nominal model parameters, defined as:

$$\hat{\tau} = \sqrt{\tau_{min}\tau_{max}} \tag{18a}$$

$$\hat{k} = \sqrt{k_{min}k_{max}} \tag{18b}$$

As Eqs. 17a and 17b show, for computing the inverse dynamics of the system, the nominal plant parameters were chosen.

The PID controller's task is to eliminate and compensate for any error due to the model inaccuracy and to deal with the process disturbances. This controller is designed on the basis of the dynamic model of the process. Since the plant output (the clad height) is proportional to the inverse of the velocity, the nonlinear memoryless block $r(\cdot)$ (see Fig. 6) placed in the feedback loop is defined as:

$$v_{PI} = r(u_{PI}) = \frac{1}{u_{PI}} \tag{19}$$

Using this block, the plant output is proportional to the control signal u_{PI}. By defining the tracking error signal as:

$$e = h_d - h \tag{20}$$

The PID control law is defined as:

$$u_{PI} = K_p\left(e + \frac{1}{60K_I}\int edt + K_d\frac{de}{dt}\right) \tag{21}$$

where K_p, K_I [min], and K_d are the proportional, integral, and derivative gains of the controller, respectively.

4 Implementation and results

4.1 Experimental setup

Several experiments were performed using a 1,000-W LASAG FLS 1042N Nd:YAG pulsed laser, a 9 MP-CL Sulzer Metco powder feeder unit, and a 3-axis CNC table. The transverse mode of the laser beam was TEM_{00} and the beam spot diameter on the workpiece was set to 1.4 mm, where the laser intensity was Gaussian.

Powder was delivered to the processing point through a lateral nozzle mounted at an angle of 30° relative to the laser beam axis. Argon gas was used for carrying the powder and also as a shield gas to shroud the melt pool. It was also used to protect the optical lenses from the flares. The shield gas flow rate was set to 3 SCFH.

Stainless steel grade 303-L powder (Fe:Cr:Ni; 70 wt%, 17 wt%, 13 wt%) with a particle size of 50 μm was chosen and sandblasted mild steel plates (0.25 C to 0.28 C; 0.6 Mn to 1.2 Mn) with dimensions of 200×30×5 m^3 were used as the substrate.

The height of the deposited metal was measured by an online processing of images taken from the process by a CCD camera [11]. Figure 7 shows a flowchart of the experimental setup.

4.2 Model identification

In order to collect data for the system identification, several single-track deposition experiments were performed using a range of different process parameters. Table 1 lists the conditions of the experiments and Fig. 8 depicts one of the experimental results. To obtain a rich set of data, we designed an experiment in which the scanning velocity was changed in a more random fashion, as shown in Fig. 8b.

According to Fig. 8a, there is no overshoot in the system response at the selected operating conditions, and the response is similar to a first-order dynamic system. Furthermore, it shows that the clad height has an inverse relationship with the velocity such that the clad height increases with decreasing velocity, and vice versa. These two effects are included in the proposed model. It has to be noted that, in this experiment, the laser was switched on at t=10 s; therefore, the model parameters were identified using the data collected at t>10 s. Further investigation of this figure indicates that there are two different response times in the rising and falling of the clad height at identical absolute velocity changes. In fact, when the clad height increases, the system is slower than for the condition when the clad height decreases. It means that the increasing rate of the clad height is smaller than the decreasing rate. For example, it takes 3.5 s to increase the clad height from 0.5 mm to 1.5 mm, but for decreasing the clad height from 1.5 mm to 0.5 mm, the required time is only 1.8 s (see Fig. 8c,d). This difference in the system response time is because of the variation in the powder catchment efficiency. With increasing powder flow rate, either the increasing rate or the decreasing rate of the clad height increases and becomes more sensitive to the velocity. At small clad heights, the melt pool is small and, therefore, the amount of powder entering the melt pool is lower than the case where the clad height is large. Consequently, the powder catchment efficiency, as well as the clad height increasing rate, is low at small clad heights. However, at large clad heights, due to the big melt pool size, the powder catchment factor is high and, as a result, the decreasing rate is high too. Another reason that may cause this different speed is the sensitivity of the clad height to the velocity. According to the proposed model, the clad height is proportional to the inverse of the

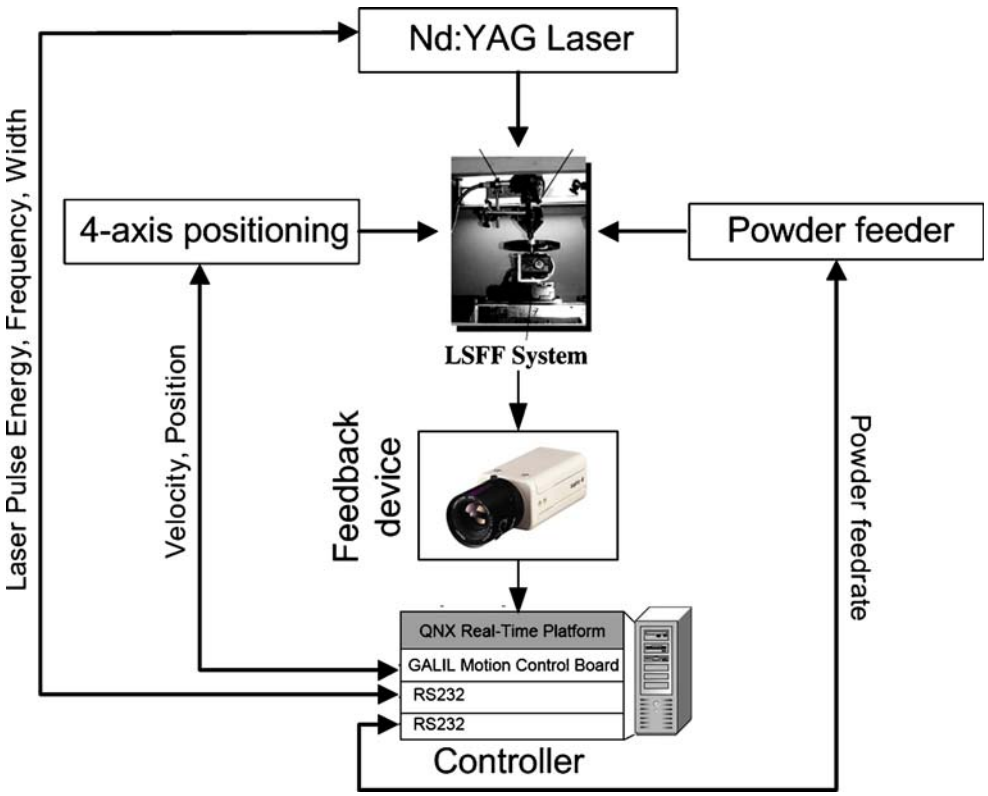

Fig. 7 Flowchart of the experimental setup

velocity; therefore, its derivation with respect to the velocity will be as follows:

$$\frac{\partial h}{\partial v} \approx -\frac{1}{v^2} \tag{22}$$

Since large clad heights occur at low velocities, the clad height is more sensitive to varying velocity when the clad height is large. It dictates that the rate of the clad height growth is lower than the rate of its decline.

Figure 9 shows the model behavior and the estimated parameters with respect to time using the RLS method. As shown, the system time constant τ changes during the process, but the parameter k remains relatively constant. The constant value of parameter k indicates the accuracy of the model in predicting the steady-state value of the clad height. According to this figure, the system time constant is different for each steady-state value of the clad height. The observed peaks are due to the identification algorithm and show the convergence speed of the algorithm to the updated value.

Offline identification resulted in the following values for the model parameters:

$$k_{min} = 0.2;\ k_{max} = 0.3;\ \tau_{min} = 0.4;\ \tau_{max} = 1.3;\ n = 3 \tag{23}$$

Table 1 Conditions of the experiments

Experiments	Conditions
Laser pulse energy	From 3 to 5 J
Laser pulse frequency	90 Hz
Laser pulse width	3 ms
Laser beam diameter	1.4 mm
Powder flow rate	2 g/min
Beam diameter (d_b)	1.4 mm
Powder jet diameter (d_p)	2 mm
Nozzle angle (α)	30°

4.3 Controller implementation

The developed feedforward PID controller was implemented on the LSFF process. Different patterns of the clad height, including step, sinusoidal, and ramp, were used in the experimental studies. To show the advantages of using the feedforward PID rather than a simple PID controller, the experimental tests were carried out in two ways: (1) PID controller without feedforward path, (2) PID controller with feedforward path.

Figure 10 shows the tracking response of the PID controller at different proportional gains and constant integral and derivative gains (K_p=0.5, 1.0, 2.0 and K_I=0.01, K_d=0.0). The figure shows that the tracking error is small and acceptable for all gains, but the tracking speed depends on the controller gains, as expected. With increasing proportional gain, the system response speed

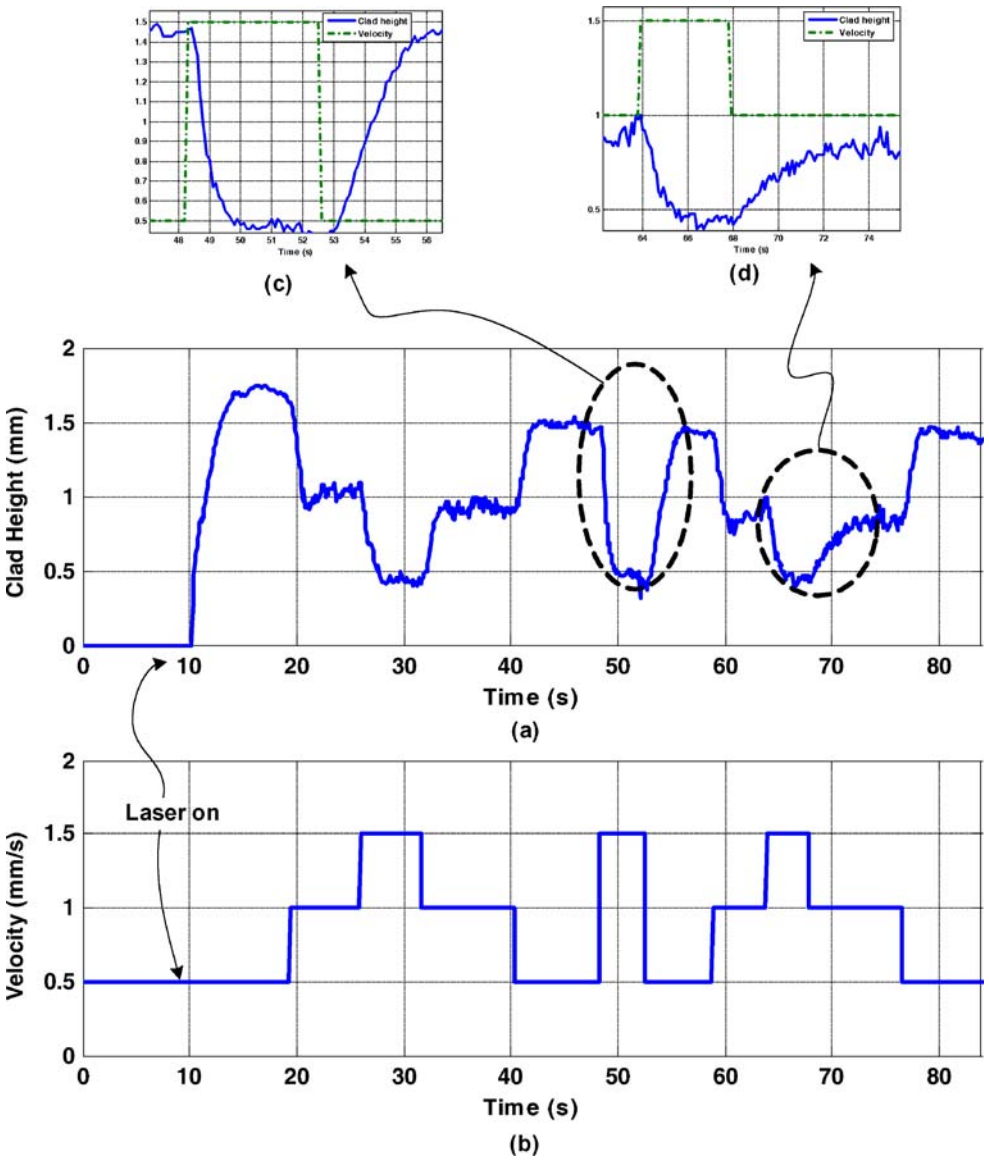

Fig. 8a–d Experimental data of the clad height variation with varying scanning velocity. **a** Actual clad height. **b** Random scanning velocity

increases; however, there is an overshoot in the clad height, which is not desirable. For example, at K_p=0.5, K_I=0.01, and K_d=0.0, the rise time is about 3 s and the clad height overshoot is limited to 0.2 mm, while at K_p=2.0, K_I=0.01, and K_d=0.0, they are 1.6 s and 0.4 mm, respectively. This indicates that having a high response speed compromises the lower overshoot value.

The performance of the PID controller at different integral gains and constant proportional and derivative gains is presented in Fig. 11. This figure shows that, with an increase in the integral gain (note that, according to Eq. 19, the integral gain K_I is proportional to the inverse of control signal), the tracking error and rise time increase, but the overshoot decreases, and vice versa. This figure also shows that, at K_I=0.005, the overshoot is about 40% and the settling time is greater than 7 s, which shows that the system response is more oscillatory; while at K_I=0.02, the overshoot becomes 20% and the settling time is 1.75 s.

In Figs. 10 and 11, it can be noted that the closed-loop system is faster when the clad decreases, as opposed to the case when it increases. This fact is due to the system behavior, as mentioned earlier. The figures also clearly illustrate that, with a simple PID controller, one cannot achieve proper response speed, small tracking error, minimum overshoot, minimum sensitivity to measurement noise, and robustness to unmodeled dynamics. For instance, with increasing the PID controller gain (in order to have a faster response), the system overshoot increases and, at high frequencies, it becomes more sensitive to measurement noises and disturbances. To overcome this problem, we used the proposed feedforward PID controller.

Figure 12 shows a comparison between the performance of the feedforward PID and the simple PID controllers. As this figure shows, although the feedforward PID controller gain is smaller than the PID controller gain, the feedforward controller is faster than the PID controller. The rise time of

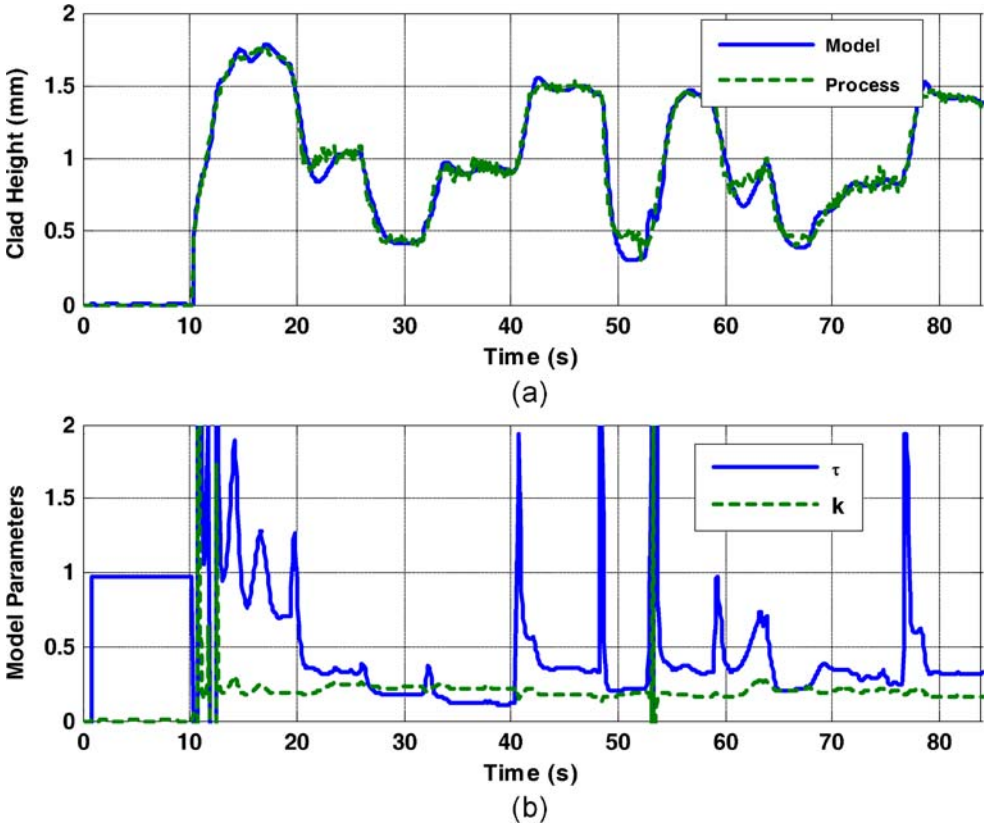

Fig. 9a, b Comparison between the identified model and the actual process responses. **a** Process and model outputs. **b** Identified values of the model parameters

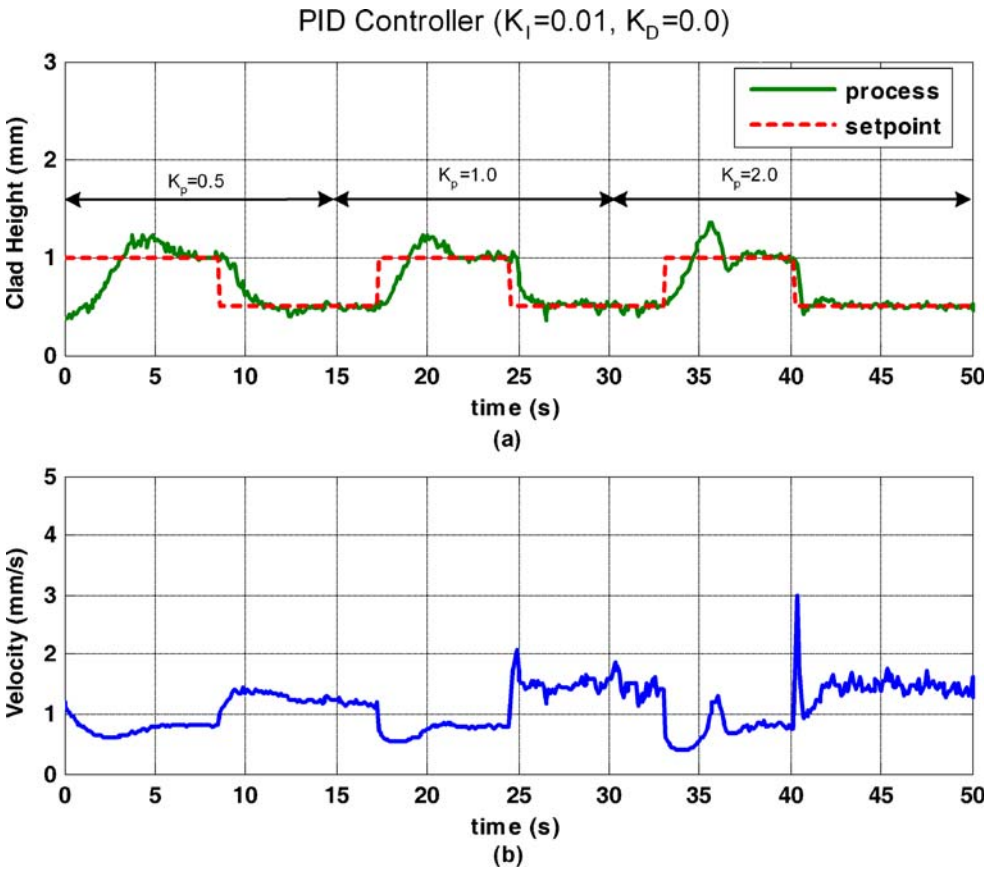

Fig. 10a, b Performance of the PID controller (without feedforward path) in following the desired clad height at different proportional gains. **a** Process output. **b** Process input

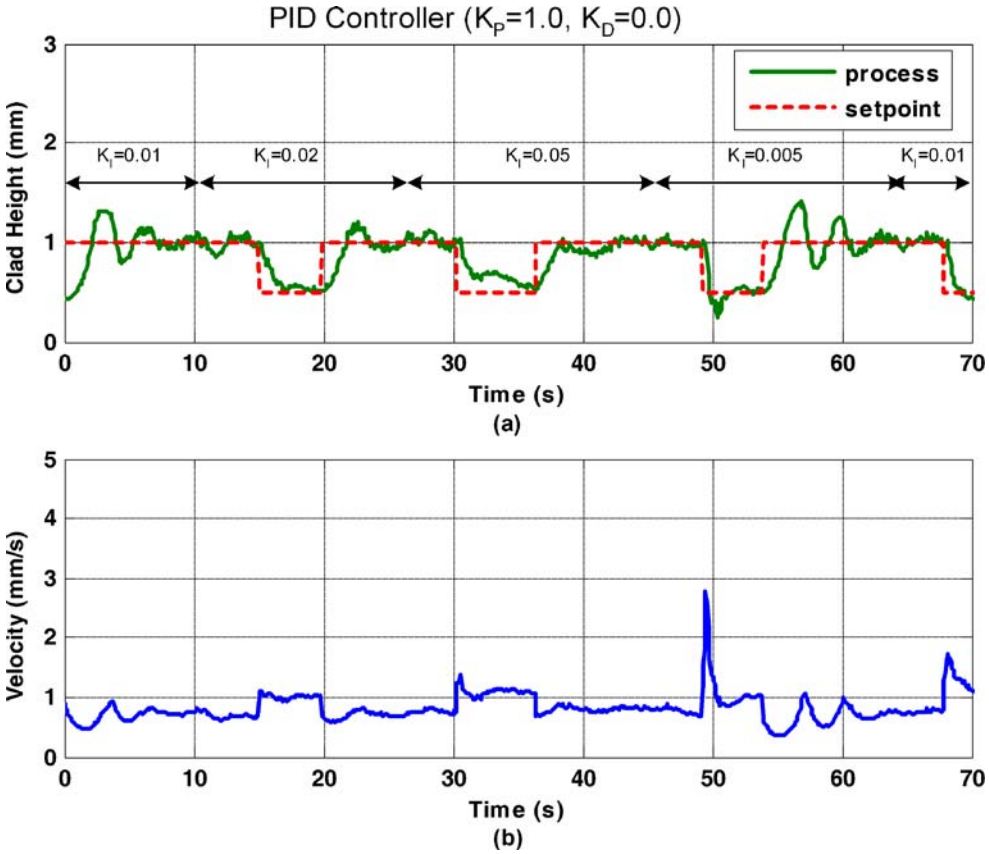

Fig. 11a, b Performance of the PID controller (without feedforward path) in following the desired clad height at different integral gains. **a** Process output. **b** Process input

the feedforward PID controller is 1.0 s, in which K_p=0.5, K_I=0.01, and K_d=0.0, while with a simple PID controller, gains of K_p=2.0, K_I=0.01, and K_d=0.0, the rise time is 1.6 s. Of interest is the fact that, although the system response speed was improved greatly (the rise time was reduced from 1.6 s to 1 s), the system overshoot did not increase and was less than 0.2 mm.

Since this thermal process is very slow, its response speed is limited and it is not possible to increase it further. Theoretically, according to Eq. 4, if the velocity goes down to zero, the clad height goes up to an infinite value with an infinite rate. But, in practice, if the velocity is zero (i.e., it is fixed), the clad height goes up with a limited rate. This limited increasing rate (i.e., approximately 1.4 mm/s in this study), which depends on the powder flow rate and the laser power, imposes a limited rise time (i.e., 1.0 s).

In the proposed feedforward PID controller, the feedforward path improves the system response speed and the PID controller reduces the tracking error and eliminates the offsets of the nominal model from the actual plant model. Moreover, the PID controller compensates for the disturbances of the process. As mentioned before, there are many sources of disturbances in this process. For example, during the LSFF process, the overall temperature of the part increases and, as a result, the laser power absorption increases and, consequently, the melt pool size changes. As another example, in multi-layer deposition, the shape of the previous layer affects the new layer geometry. In this case, the shape of the previous layer, in fact, acts as a disturbance for the new layer. The proposed controller is able to compensate for this kind of disturbance and is able to deposit a layer with a desired shape on a substrate with a nonplanar surface.

Figure 13 shows a case in which a clad with a constant height was deposited on a substrate with two slots. The depth of each slot was 0.5 mm and its width was 12.5 mm. The goal of this experiment was to maintain the clad height at a constant value of 0.5 mm relative to the substrate under geometrical disturbances. As this figure illustrates, the controller decreases the velocity when the process reaches the slot such that the clad height from the original substrate surface remains constant. Due to the system response speed, the clad height at the beginning point of the slot is smaller than the desired value and there is an overshoot at the ending point of the slot.

In order to investigate the capability of the developed feedforward PID controller in the production of a part, a test was carried out to generate a sinusoidal shape as shown in Fig. 14. Figure 14a shows that the closed-loop system followed the setpoint with very good accuracy. Figure 14b,c shows two views of the sinusoidal surface fabricated by the proposed closed-loop system. As seen, a good dimen-

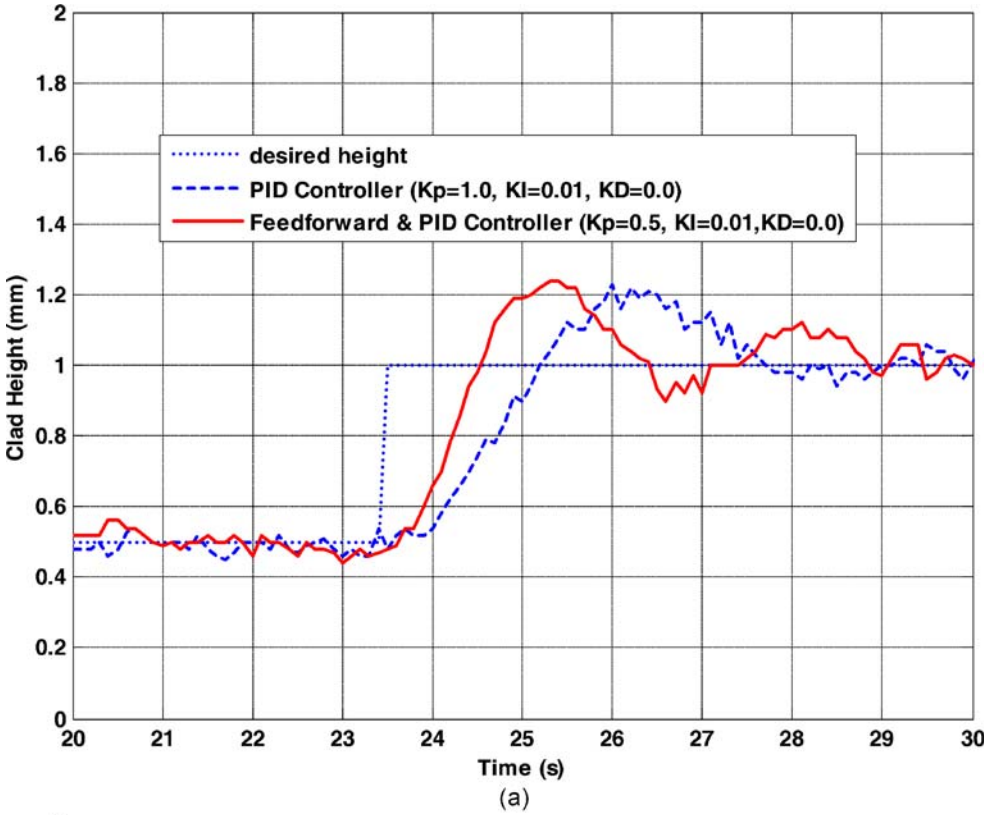

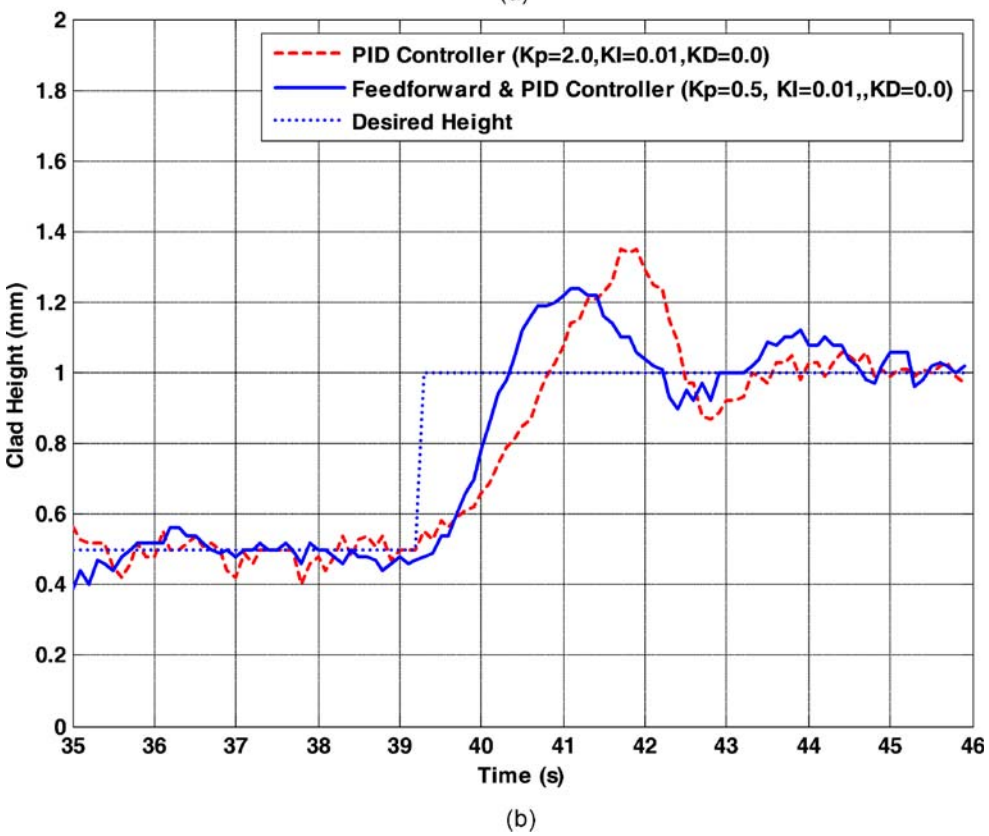

Fig. 12a, b Comparison between the feedforward PID controller and the simple PID controller at different PID controller gains. **a** K_p=1.0, K_I=0.01, K_d=0. **b** K_p=2.0, K_I=0.01, K_d=0 (feedforward PID controller gains were kept constant)

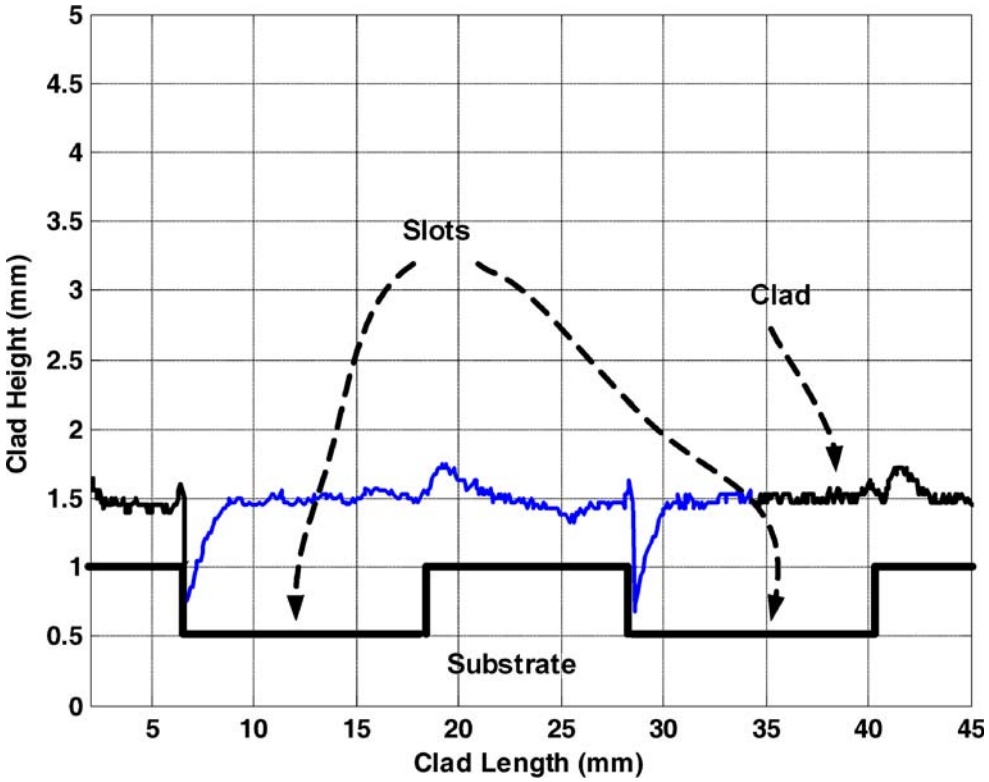

Fig. 13 Controller performances in compensating for the effects of the substrate shape on the clad height

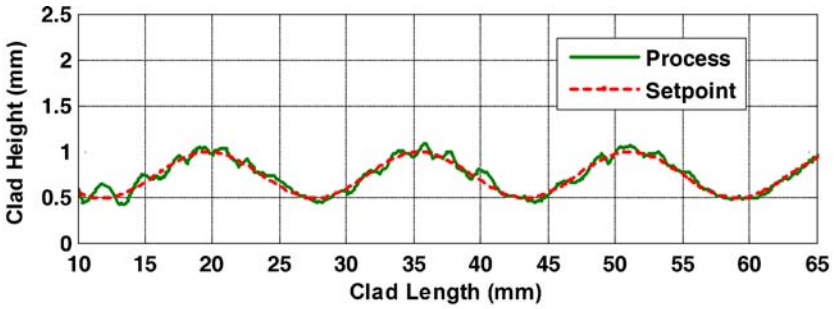

(a)

(b)

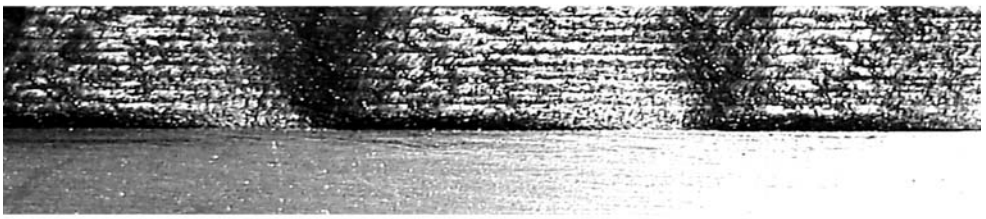

(c)

Fig. 14a–c Closed-loop system performance in depositing a sinusoidal shape. **a** Process output and setpoint. **b** Side view. **c** Top view

sional accuracy has been obtained, in which the average of the tracking error is about 2%.

5 Conclusion

A feedforward proportional-integral-derivative (PID) controller was developed for the laser solid freeform fabrication (LSFF) process. The controller was designed based on a semi-empirical nonlinear model. The proposed model relates the scanning velocity to the clad height. The controller uses the velocity for compensating for the deviation of the clad height from the preset value. Using the experimental assessments, the unknown model parameters were identified offline. The identification results showed that, when the clad height increases, the system response speed is lower compared to the condition when the clad height decreases. Moreover, it was shown that the feedforward PID controller can effectively control the process with a good dimensional accuracy compared to a simple PID controller, resulting in lower response times and overshoot. The capability of the proposed controller in the production of a part was assessed with the fabrication of a nonplanar surface.

References

1. Vilar R (1999) Laser cladding. J Laser Appl 11(2):64–79
2. Jeng JY, Lin MC (2001) Mold fabrication and modification using hybrid processes of selective laser cladding and milling. J Mater Process Technol 110(1):98–103
3. Hu D, Kovacevic R (2003) Sensing, modeling and control for laser-based additive manufacturing. Int J Mach Tools Manuf 43(1):51–60
4. Mazumder J, Schifferer A, Choi J (1999) Direct materials deposition: designed macro and microstructure. Mater Res Innov 3(3):118–131
5. Liu J, Li L (2004) In-time motion adjustment in laser cladding manufacturing process for improving dimensional accuracy and surface finish of the formed part. Opt Laser Technol 36(6):477–483
6. Hua Y, Choi J (2005) Adaptive direct metal/material deposition process using a fuzzy logic-based controller. J Laser Appl 17 (4):200–210
7. Toyserkani E, Khajepour A, Corbin SF (2002) Application of experimental-based modeling to laser cladding. J Laser Appl 14 (3):165–173
8. Römer GRBE, Aarts RGKM, Meijer J (1999) Dynamic models of laser surface alloying. Lasers Eng 8(4):251–266
9. Nelles O (2000) Nonlinear system identification. Springer, Berlin Heidelberg New York, ISBN 3-540-67369-5
10. Frenk A, Vandyoussefi M, Wagniere JD, Zryd A, Kurz, W (1997) Analysis of the laser-cladding process for stellite on steel. Metall Mater Trans B—Proc Metall Mater Proc Sci 28(3):501–508
11. Toyserkani E, Khajepour A, Corbin SF (2003) Vision-based feedback control of laser powder deposition. In: Billingsley J (ed) Mechatronics and machine vision 2003 (M2VIP2003): future trends, RSP Press, Great Britain, ISBN 0-8638-0290-7